Supplement of Atmos. Chem. Phys., 22, 4101–4116, 2022
https://doi.org/10.5194/acp-22-4101-2022-supplement

Atmospheric Chemistry and Physics
Open Access

Supplement of

Impacts of aerosol–photolysis interaction and aerosol–radiation feedback on surface-layer ozone in North China during multi-pollutant air pollution episodes

Hao Yang et al.

Correspondence to: Lei Chen (chenlei@nuist.edu.cn) and Hong Liao (hongliao@nuist.edu.cn)

Table S1. Locations of the ten stations from NOAA's National Climatic Data Center used in this study.

Station	Latitude (°)	Longitude (°)
Yuxian	39.833	114.567
Fengning	41.2	116.633
Zhangjiakou	40.783	114.883
Huailai	40.417	115.5
Chengde	40.967	117.917
Beijing	40.08	116.585
Tianjin	39.1	117.167
Binhai	39.124	117.346
Tangshan	39.65	118.1
Baoding	38.733	115.483

Table S2. Locations of the thirty-two stations from China National Environmental Monitoring Center used in this study.

Station	Latitude (°)	Longitude (°)
Beijing_1	39.8673	116.366
Beijing_2	40.2865	116.17
Beijing_3	39.9522	116.434
Beijing_4	39.8745	116.434
Beijing_5	39.9716	116.473
Beijing_6	39.9425	116.361
Beijing_7	39.9934	116.315
Beijing_8	40.1438	116.72
Beijing_9	40.3937	116.644
Beijing_10	40.1952	116.23
Beijing_11	40.0031	116.407
Beijing_12	39.9279	116.225
Tianjin_1	39.097	117.151
Tianjin_2	39.173	117.193
Tianjin_3	39.1654	117.145
Tianjin_4	39.1205	117.184
Tianjin_5	39.1082	117.237
Tianjin_6	39.0927	117.202
Tianjin_7	39.2133	117.1837
Tianjin_8	39.1337	117.269
Tianjin_9	39.0877	117.307
Tianjin_10	39.0343	117.707
Tianjin_11	38.8394	117.457
Tianjin_12	39.124	117.401
Tianjin_13	39.1587	117.764
Tianjin_14	38.9194	117.157
Baoding_1	38.8632	115.493
Baoding_2	38.8957	115.5223
Baoding_3	38.9108	115.4713
Baoding_4	38.8416	115.4612
Baoding_5	38.8756	115.442
Baoding_6	38.8707	115.5214

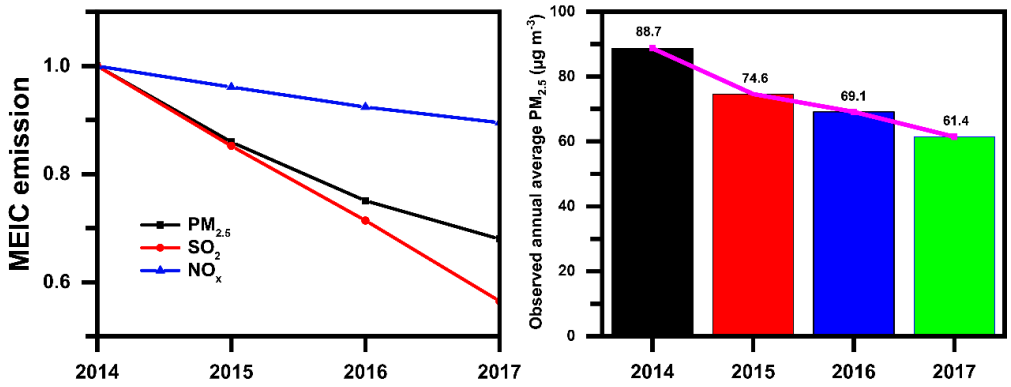

Figure S1. Trends of emissions over 2014–2017 from MEIC emission inventory and the observed annual mean $PM_{2.5}$ concentrations in the studied domain during 2014-2017.

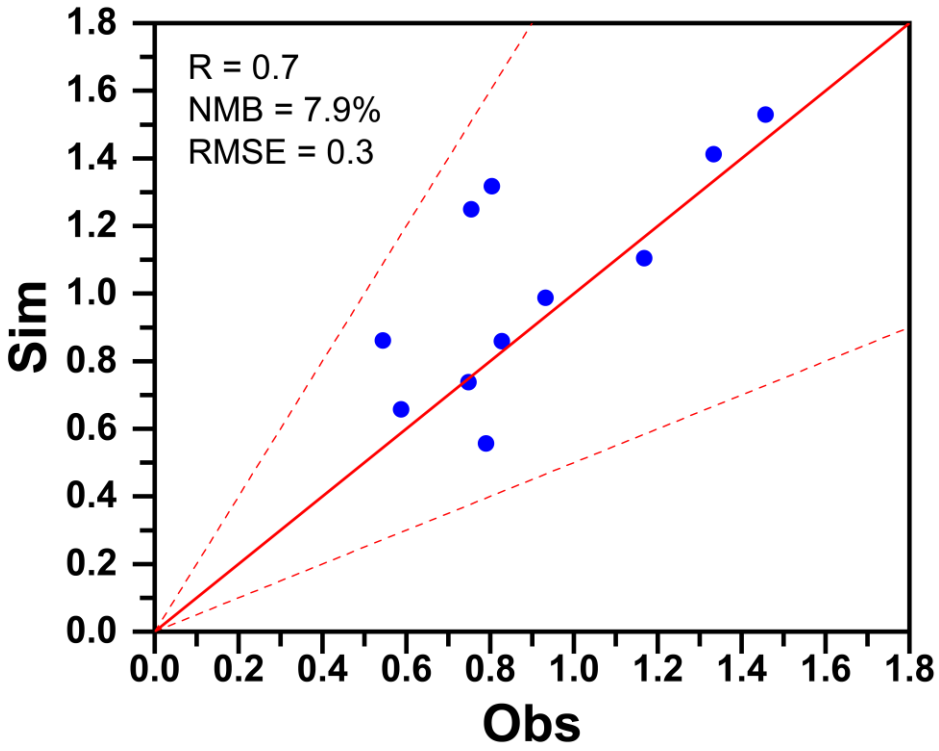

Figure S2. Comparison of observed and simulated AOD at 550 nm in Beijing (39.98°N, 116.38°E). The observed AOD during the four episodes are collected from AERONET.

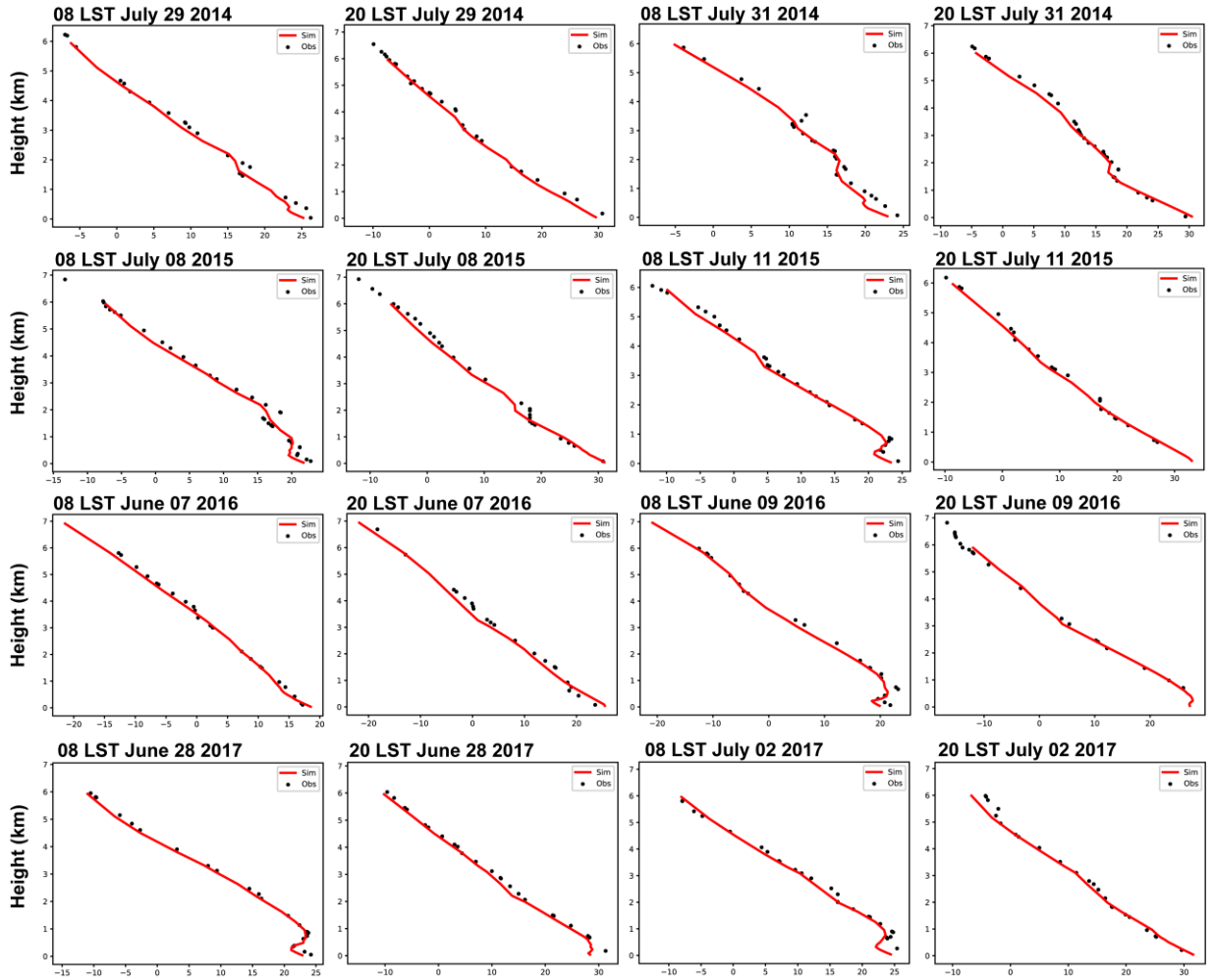

Figure S3. Observed (black dots) and simulated (red lines) temperature profiles at 08:00 and 20:00 LST in Beijing (39.93°N, 116.28°E) during the four episodes.

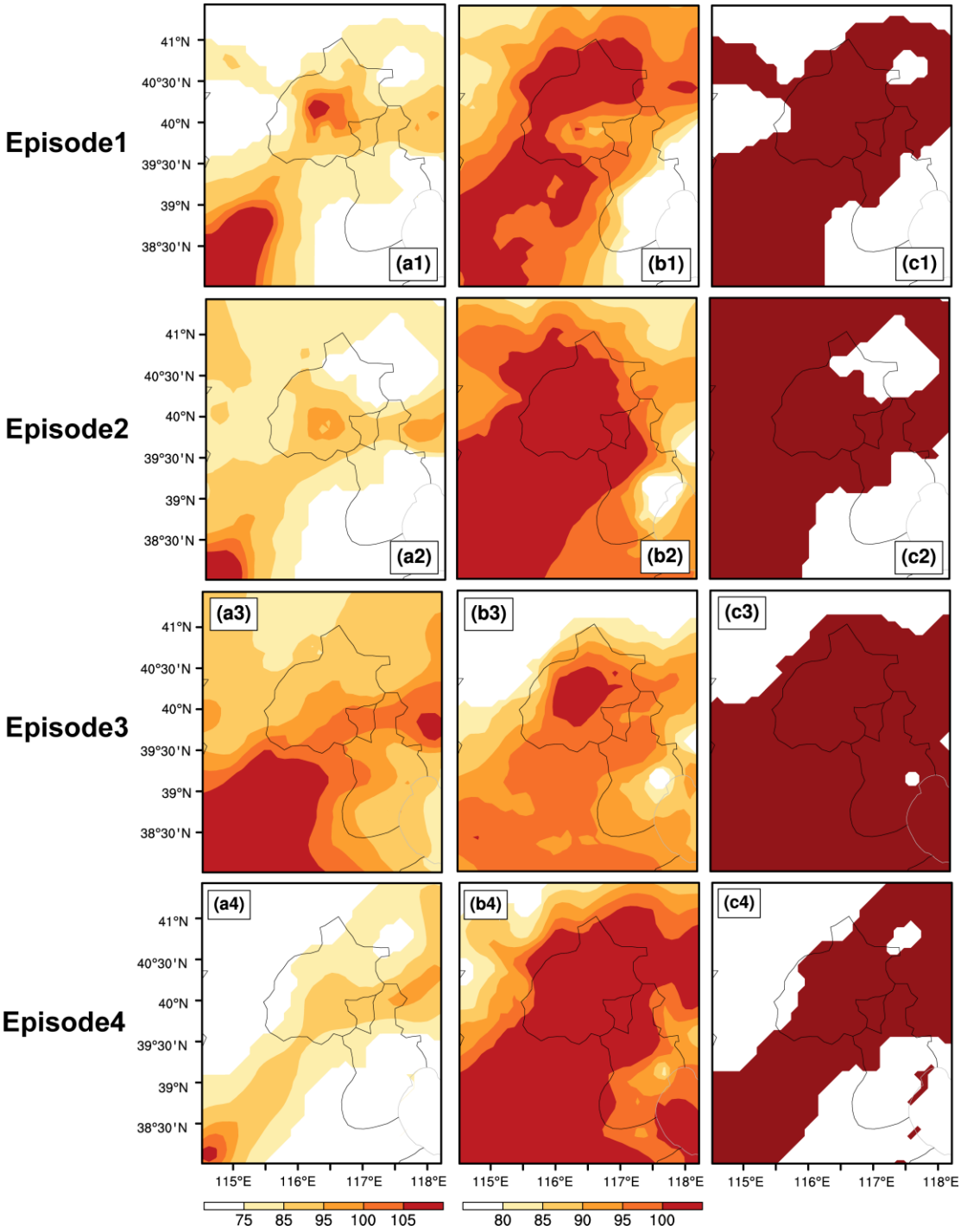

Figure S4. The spatial distributions of simulated (a) $PM_{2.5}$ (μg m^{-3}) and (b) MDA8 O_3 (ppb) concentrations during 28 July to 3 August 2014 (Episode1), 8-13 July 2015 (Episode2), 5-11 June 2016 (Episode3) and 28 June to 3 July 2017 (Episode4). (c) The defined complex air pollution areas (CAPAs, shaded by red) where $PM_{2.5}$ and MDA8 O_3 concentrations are larger than 75 μg m^{-3} and 80 ppb, respectively.

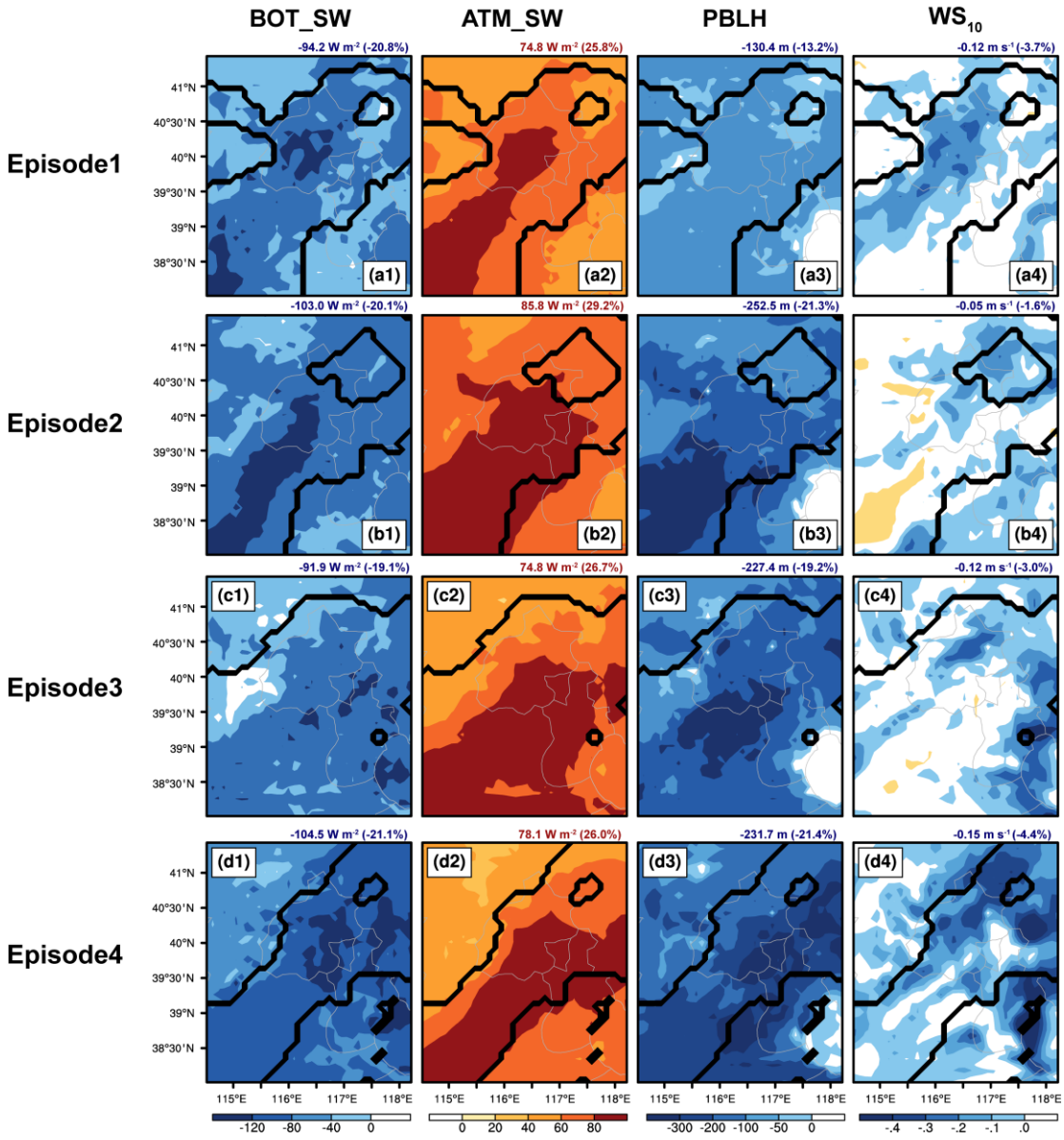

Figure S5. Changes in shortwave radiation at the surface (BOT_SW), shortwave radiation in the atmosphere (ATM_SW), PBL height (PBLH), and 10-m wind speed (WS_{10}) caused by ARF in the daytime (08:00-17:00 LST) during 28 July to 3 August 2014 (Episode1), 8-13 July 2015 (Episode2), 5-11 June 2016 (Episode3) and 28 June to 3 July 2017 (Episode4). The calculated changes (percentage changes) averaged over CAPAs are also shown at the top of each panel.

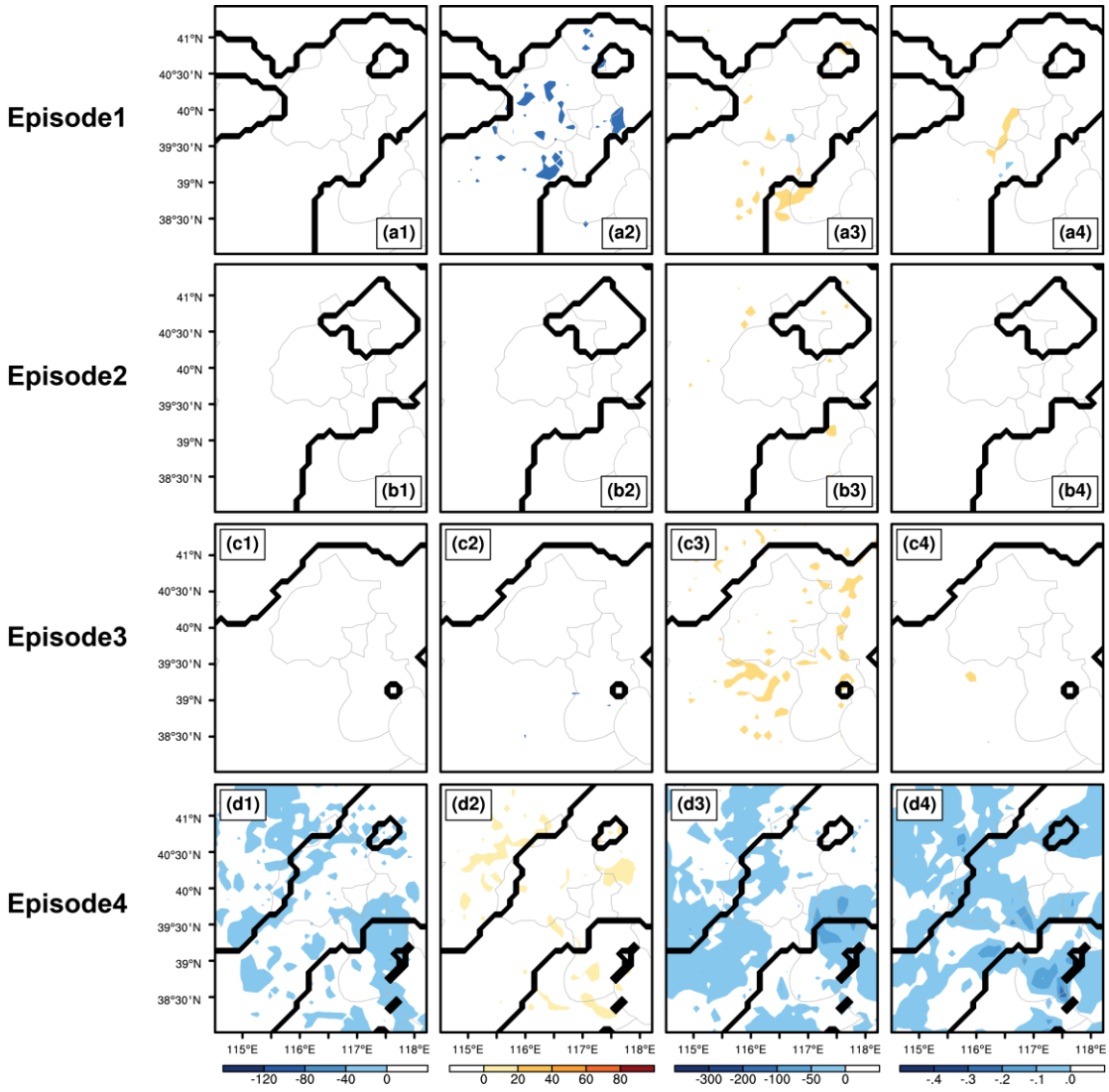

Figure S6. Changes in shortwave radiation at the surface (BOT_SW), shortwave radiation in the atmosphere (ATM_SW), PBL height (PBLH), and 10-m wind speed (WS_{10}) caused by API during the daytime (08:00-17:00 LST) during 28 July to 3 August 2014 (Episode1), 8-13 July 2015 (Episode2), 5-11 June 2016 (Episode3) and 28 June to 3 July 2017 (Episode4).

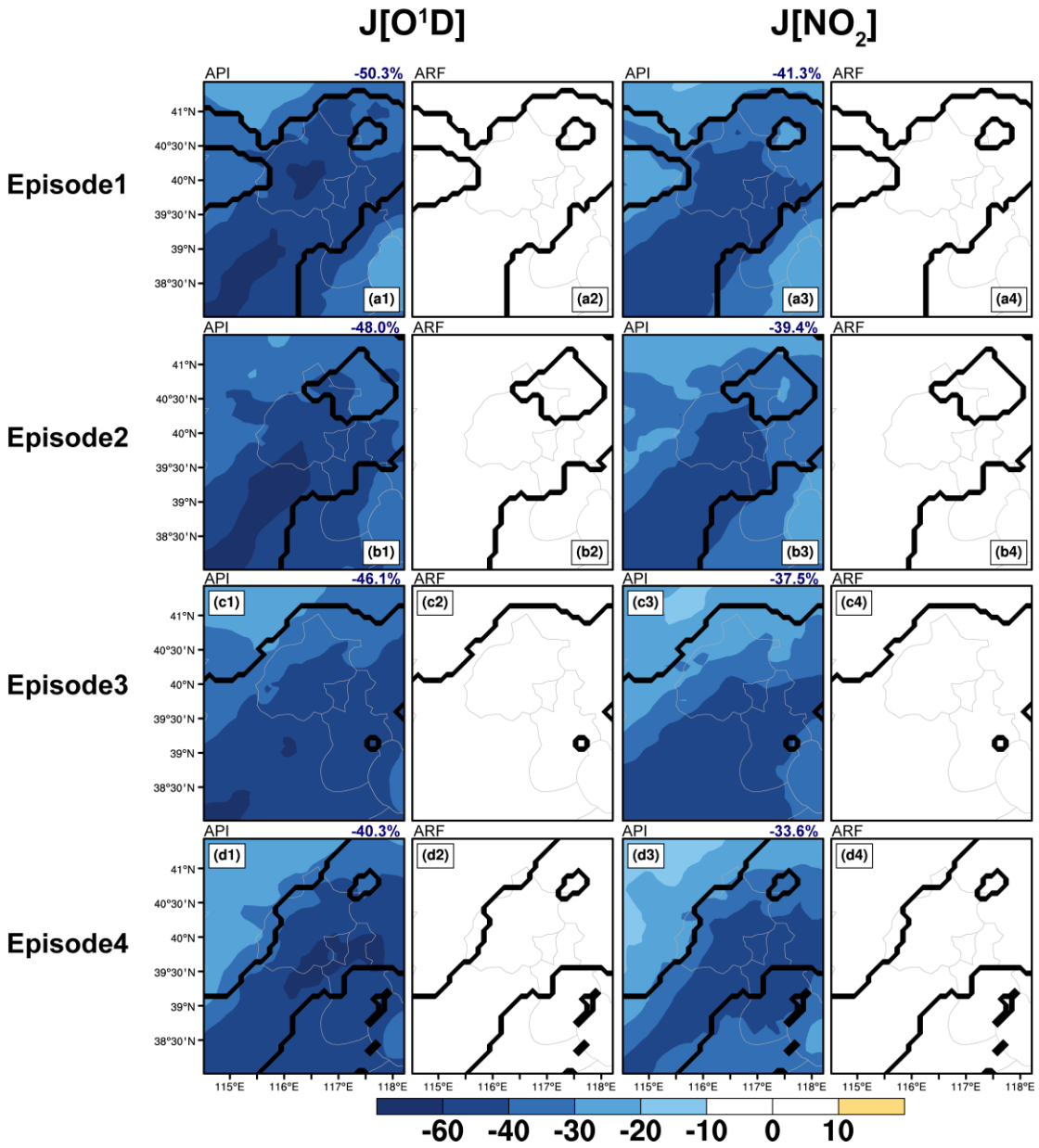

Figure S7. Percentage changes in (a-b) J[O^1D] and (c-d) J[NO_2] caused by API and ARF during the daytime (08:00-17:00 LST) during 28 July to 3 August 2014 (Episode1), 8-13 July 2015 (Episode2), 5-11 June 2016 (Episode3) and 28 June to 3 July 2017 (Episode4). The calculated changes averaged over CAPAs are also shown at the top of each panel.

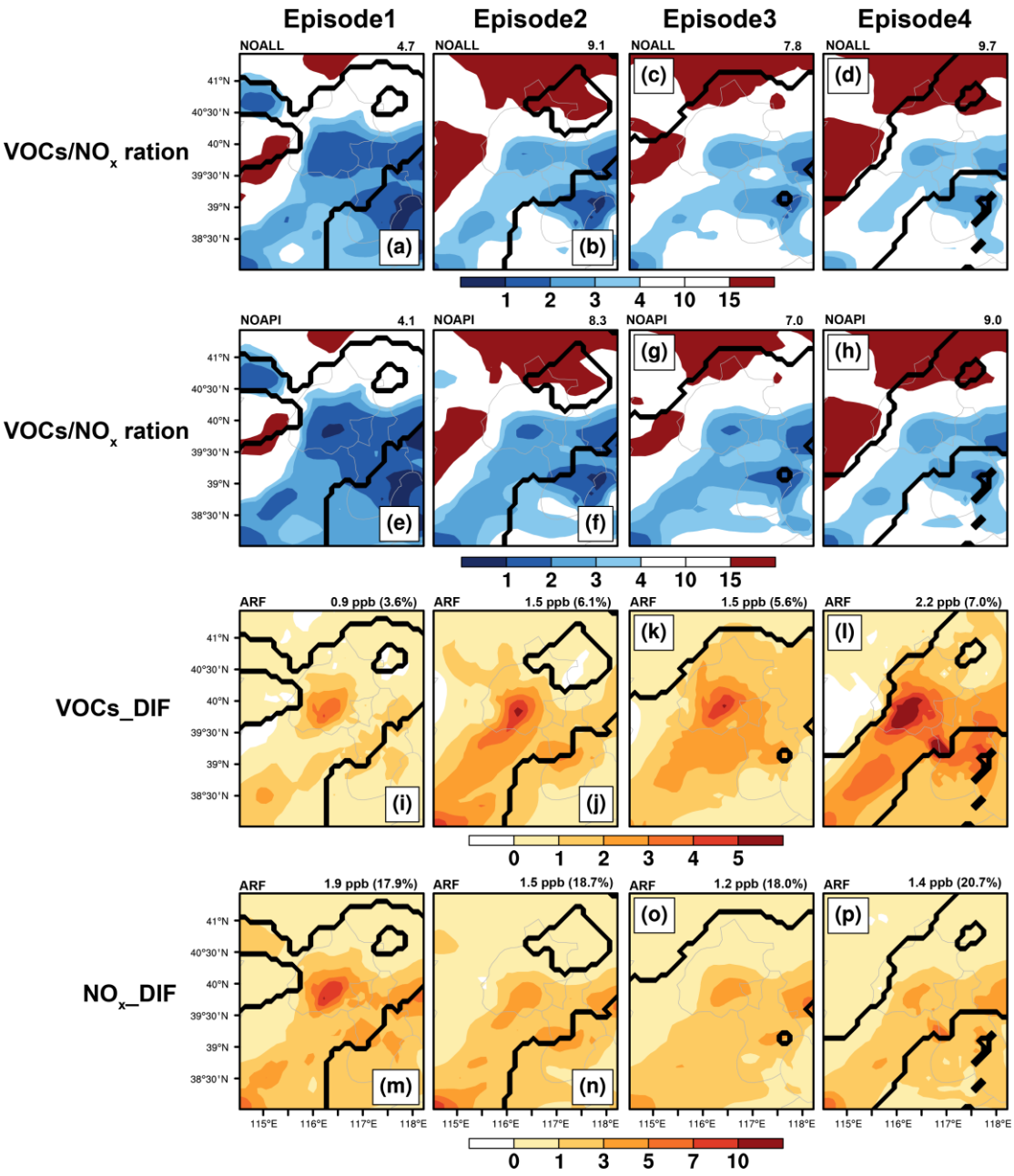

Figure S8. The ratios of VOCs/NO_x calculated from (a-d) NOALL, and (e-h) NOAPI. The changed surface-layer concentrations of (i-l) VOCs and (m-p) NO_x (NO_2+NO, ppb) caused by ARF during the daytime (08:00-17:00 LST) from Episode1 to Episode4. The calculated values averaged over CAPAs are also shown at the top of each panel.

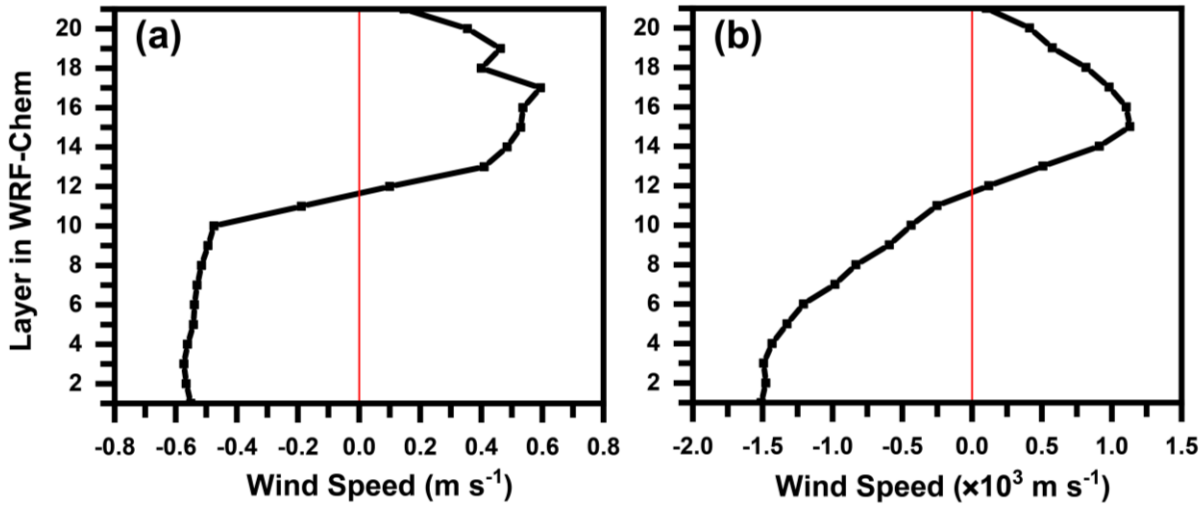

Figure S9. The impacts of ARF on (a) horizontal and (b) vertical wind speed in different model layers averaged over CAPAs in the daytime (08:00-17:00 LST) during the four episodes.

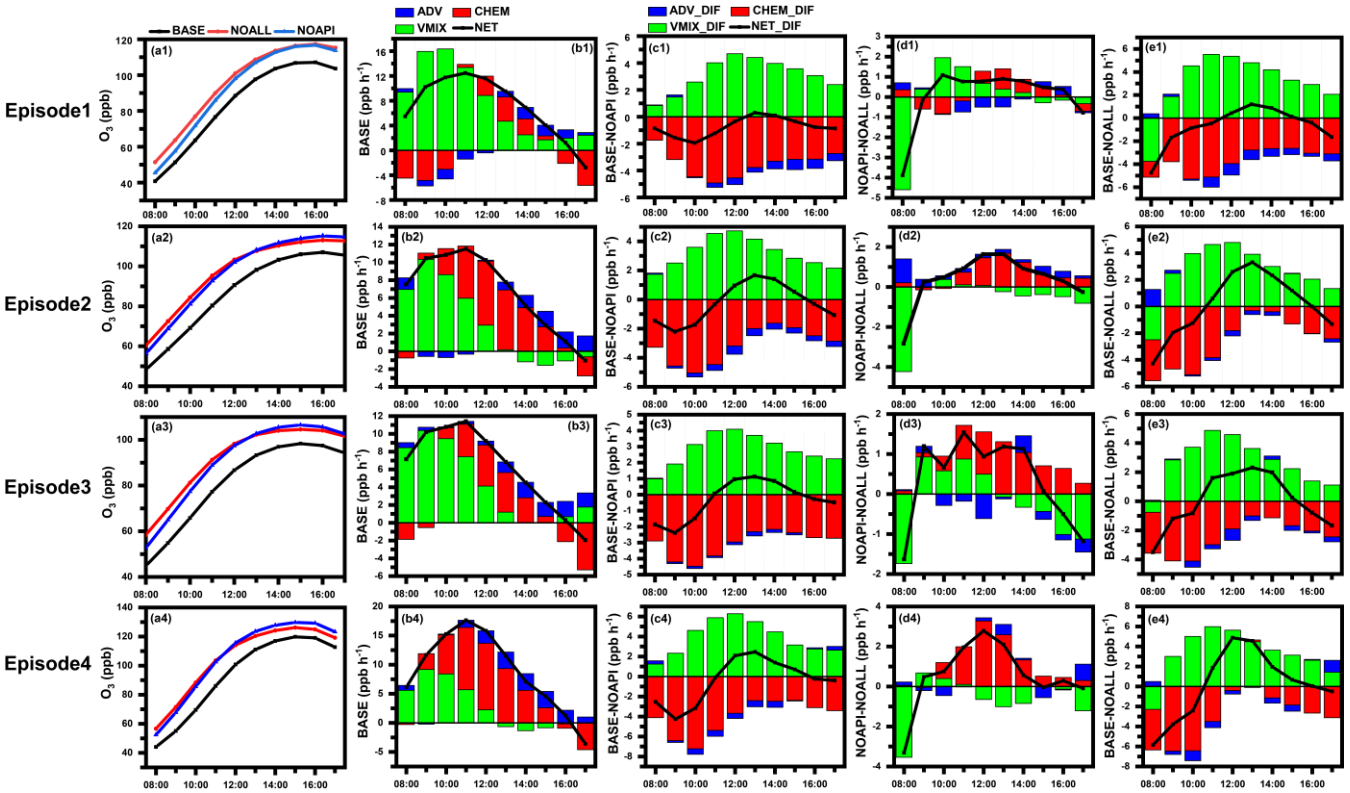

Figure S10. Temporal evolution characteristics of aerosol-radiation interactions on O_3 for the four episodes. (a) Diurnal variations of simulated surface O_3 concentrations in BASE (black dotted line), NOAPI (blue dotted line), and NOALL (red dotted line) cases over CAPAs. (b) Hourly changes in surface O_3 induced by each physical/chemical process using the IPR analysis in BASE case. Changes in hourly surface O_3 process contributions caused by (c) API, (d) ARF, and (e) ALL over CAPAs during the daytime (08:00-17:00 LST). The black lines with squares denote the net contribution of all processes (NET, defined as VMIX+CHEM+ADV). Differences of each process contribution are denoted as VMIX_DIF, CHEM_DIF, ADV_DIF, and NET_DIF.

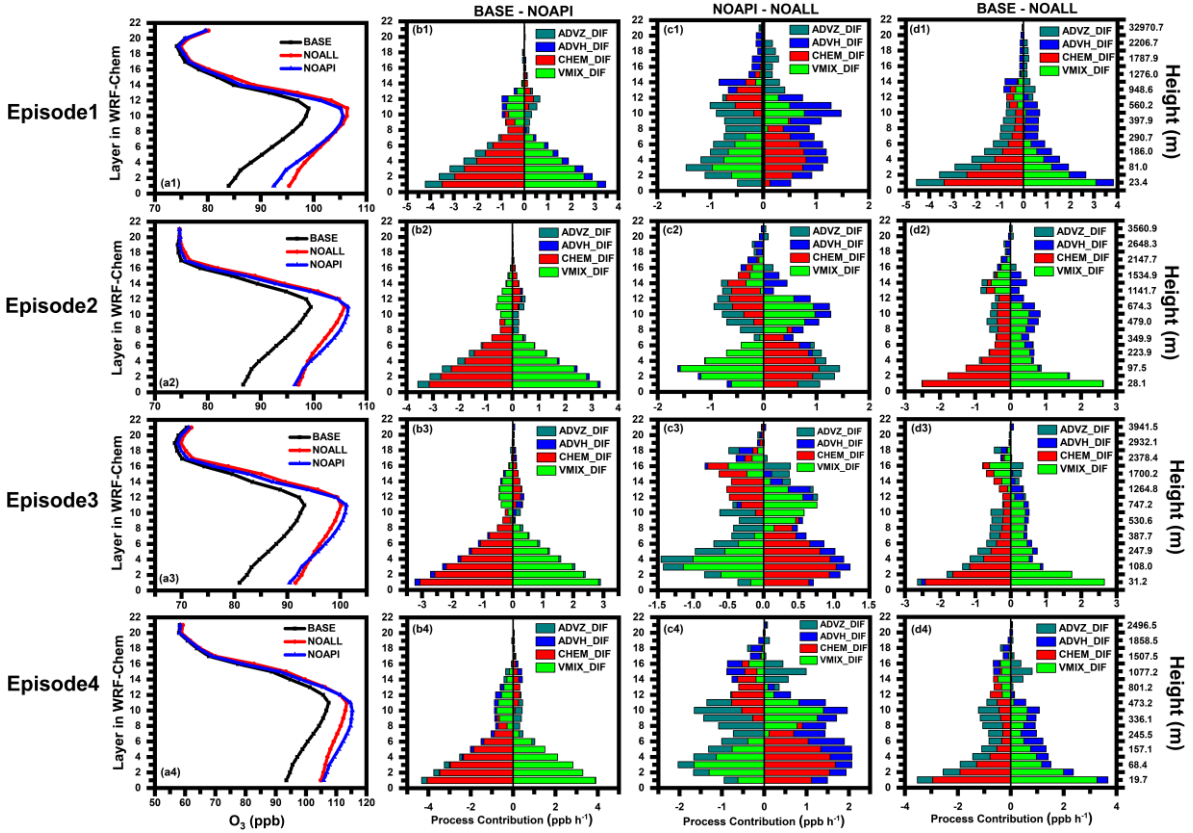

Figure S11. The impacts of aerosol-radiation interactions on vertical O_3 for the four episodes. (a) Vertical profiles of simulated O_3 concentrations in BASE (black dotted line), NOAPI (blue dotted line), and NOALL (red dotted line) cases over CAPAs. Changes in O_3 budget due to (b) API, (c) ARF, and (d) ALL over CAPAs during the daytime (08:00-17:00 LST). Differences of each process contribution are denoted by ADVZ_DIF, ADVH_DIF, CHEM_DIF, and VMIX_DIF.

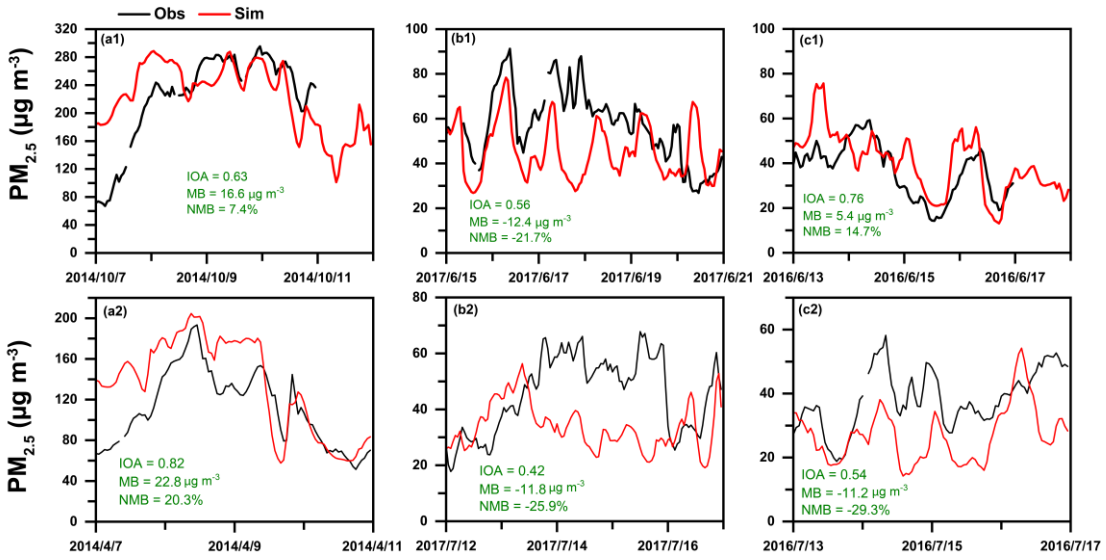

Figure S12. Time series of observed (black) and simulated (red) hourly surface-layer $PM_{2.5}$ concentrations averaged over the thirty-two observation sites in Beijing, Tianjin, and Baoding during 7-12 October 2014 (High_PM_Episode1), 7-11 April 2014 (High_PM_Episode2), 15-21 June 2017 (High_O_3_Episode1), 12-17 July 2017 (High_O_3_Episode2), 13-18 June 2016 (Low_POL_Episode1), and 13-17 July 2016 (Low_POL_Episode2). The index of agreement (IOA), mean bias (MB), and normalized mean bias (NMB) are also shown.

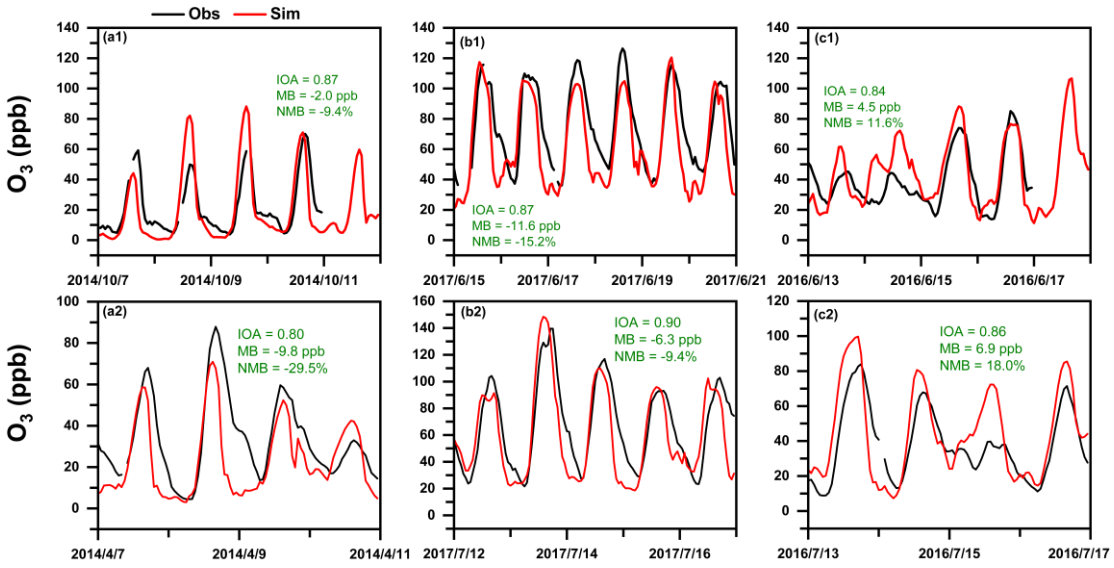

Figure S13. The same as Fig. S12, but for O_3.